Emerging satellite observations for diurnal cycling of ecosystem processes Jingfeng Xiao^{1*}, Joshua B. Fisher², Hirofumi Hashimoto^{3, 4}, Kazuhito Ichii⁵, Nicholas C. Parazoo² ¹Earth Systems Research Center, Institute for the Study of Earth, Oceans, and Space, University of New Hampshire, Durham, NH, USA ²Jet Propulsion Laboratory, California Institute of Technology, Pasadena, CA, USA ³Department of Applied Environmental Science, California State University – Monterey Bay, Seaside, CA, USA ⁴NASA Ames Research Center, Moffett Field, CA, USA ⁵Center for Environmental Remote Sensing, Chiba University, Chiba, Japan *Correspondence to: j.xiao@unh.edu

Abstract:

24

25

26

27

28

29

30

31

32

33

34

35

36

37

38

39

40

41

42

43

44

Diurnal cycling of plant carbon uptake and water use, and their responses to water and heat stresses, provide direct insight for assessing ecosystem productivity, agricultural production and management practices, carbon and water cycles, and feedbacks to the climate. Temperature, light, atmospheric water demand, soil moisture, and leaf water potential vary over the course of the day, leading to diurnal variations in stomatal conductance and ecosystem processes. Earth observations from polar-orbiting satellites are incapable of studying these diurnal variations. We review the emerging satellite observations that have the potential for studying how plant functioning and ecosystem processes vary over the course of the diurnal cycle. The recently launched ECOsystem Spaceborne Thermal Radiometer Experiment on Space Station (ECOSTRESS) and Orbiting Carbon Observatory-3 (OCO-3) provide land surface temperature (LST), evapotranspiration (ET), and solar-induced fluorescence (SIF) data at different times of day. New generation operational geostationary satellites such as Himawari-8 and the GOES-R series can provide continuous, highfrequency data of LST, solar radiation, and gross primary production (GPP). Future satellite missions such as GeoCarb, TEMPO, and Sentinel-4 are also planned to have diurnal SIF sampling capability. We explore the unprecedented opportunities for characterizing and understanding how GPP, ET, and water use efficiency (WUE) vary over the course of the day in response to temperature and water stresses and management practices. We also envision that these emerging observations will revolutionize studies of plant functioning and ecosystem processes in the context of climate change and that these observations and findings can inform agricultural and forest management and lead to improvement of Earth system models and climate projections.

- 45 **Keywords:** Plant functioning; photosynthesis; evapotranspiration; water use efficiency; circadian
- 46 rhythms; stomatal conductance

Plant scientists and ecologists have been intrigued by the circadian rhythms (i.e., circadian clock) of plants for decades ^{1,2}. Many compelling science questions have arisen regarding the diurnal (i.e. diel) patterns of plant photosynthesis and transpiration. For example, how do plants use resources throughout the day? How does stomatal conductance change in response to environmental and internal factors (e.g., air temperature, light, atmospheric water demand, soil moisture, and leaf water potential/storage)? How do plant photosynthesis, transpiration, and water use efficiency (WUE) respond to these environmental factors? Addressing these questions is increasingly important in the context of climate change. Increasing water and heat stresses ^{3,4} can have large impacts on plant functioning and ecosystem processes, particularly during the midday period; plants may exhibit more frequent stomatal closure and midday depression, which can have significant impacts on plant growth, carbon uptake, and plant survival. Better understanding the responses of plants to water and heat stresses over the course of the day is critical for assessing the impacts of drought and heat waves on plant production and survival, food security, and terrestrial carbon dynamics and projecting carbon-climate feedbacks.

Elucidating diurnal cycling of plant water loss by transpiration and carbon gain by photosynthesis is of fundamental importance for understanding how plants interact with ambient and changing environmental conditions. Dissymmetric evolution of stomatal conductance and midday stomatal closure have been shown for different plant species, life stages, ecosystems ^{5,6,7}. As a result, photosynthesis can exhibit an afternoon decline and a midday depression (Fig. 1) ^{8,9,10}, leading to a two-peaked and dissymmetric diurnal pattern ¹¹. The diurnal variations of stomatal conductance also shape the diurnal pattern of transpiration (Fig. 1). Water stress might result in a larger decrease in evapotranspiration (ET) than in gross primary production (GPP), leading to higher WUE ¹². Water stress may also decrease WUE and lead to less efficient carbon uptake.

Diurnal patterns of stomatal conductance, ET, and GPP may exhibit large differences among different plant and ecosystem types. Better understanding diurnal courses of plant water use and carbon uptake is essential for understanding the relations between water and productivity of natural and managed ecosystems ¹¹, providing insight into the vulnerability and resilience of different ecosystems to drought and/or heat stress ¹³, and informing management practices (e.g., irrigation).

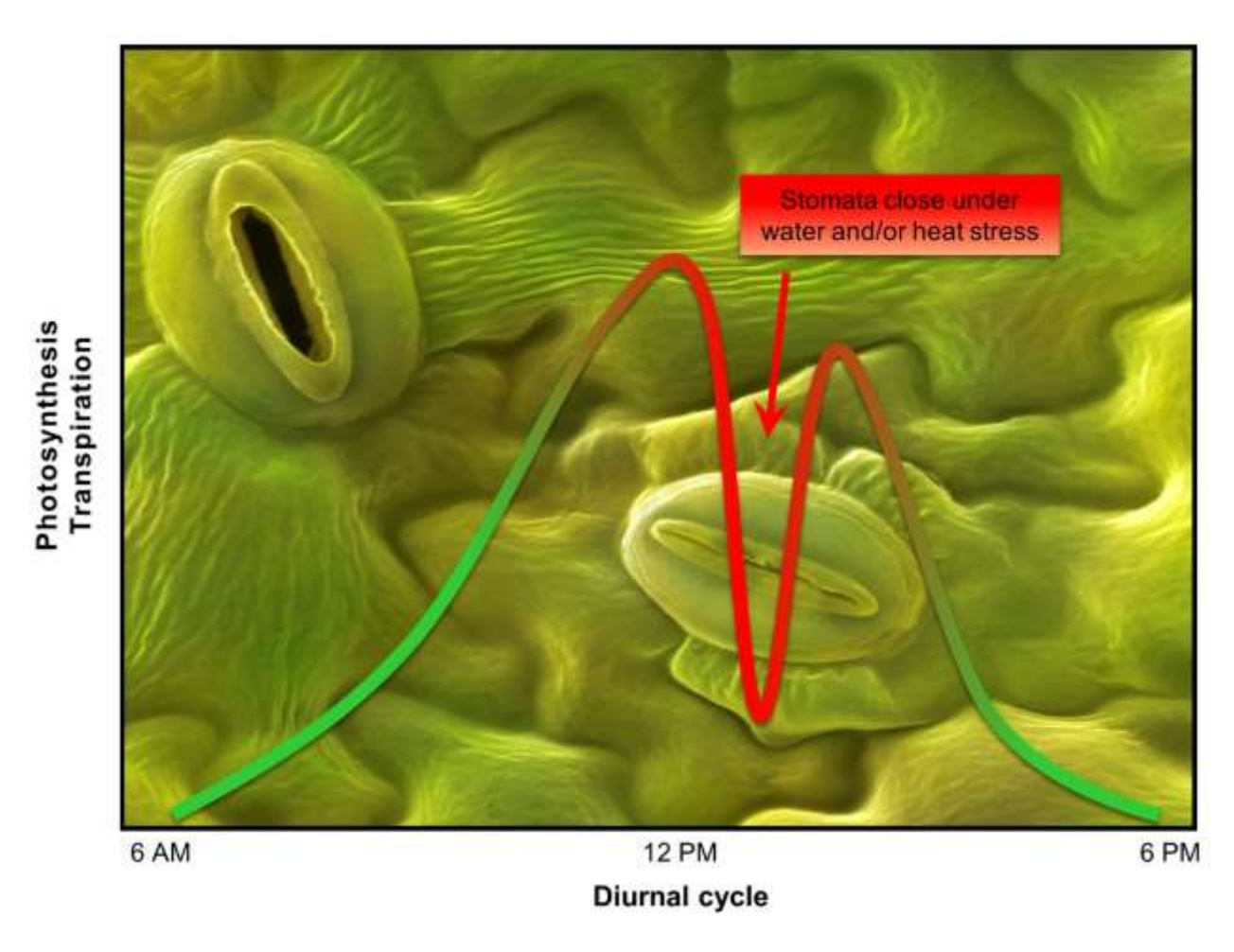


Fig. 1 Conceptual diagram of plant photosynthesis and transpiration over the course of a day. Both transpiration and photosynthesis may show mid-afternoon depressions due to stomatal closure under water and/or heat stresses. The background image shows open and closed stomata on a lavender leaf (Lavendula dentata), colored scanning electron micrograph (SEM) (Source: Science Photo Library; magnification ×2000 at an image size of 10 cm wide). Stomata are pores on leaves that open and close to regulate the exchange of gases (carbon dioxide, water).

Observations at multiple times of the day are essential for understanding the diurnal cycles of plant water use and carbon uptake. At canopy and ecosystem scales, in-situ measurements with portable instruments ¹⁴ and the eddy covariance (EC) technique ^{15, 16} have been widely used to examine the diurnal variations of plant functioning and ecosystem processes. In particular, the EC sites provide continuous, sub-hourly measurements of ecosystem carbon and water exchange, meteorological variables, and soil moisture ¹⁷, allowing scientists to analyze how stomatal conductance, photosynthesis, and transpiration vary over the course of the diurnal cycle ^{15, 16}. However, these in-situ measurements are spatially sparse, and the resulting findings do not necessarily apply elsewhere.

Compared with in-situ techniques, satellites can provide direct observations of plants over regions or the globe. Satellites measure plant status, canopy cover, plant productivity, vegetation structure, water stress, and other plant or environmental variables. Earth observations from polar-orbiting satellites such as Landsat, Sentinel, Terra, Aqua, and Orbiting Carbon Observatory-2 (OCO-2) have been widely used to examine ecosystem processes (e.g., GPP, ET, WUE) at regional to global scales ^{18, 19, 20, 21}. However, polar-orbiting satellites typically acquire at best one or two snapshots of a given location during each day or a certain period (e.g., 16 days), at the same time of the day/night, and therefore are not designed to study diurnal variations of plant water use and carbon uptake. The carbon and water flux datasets based on these satellite data are available at daily or longer (e.g., 8-day) timescales (e.g., global GPP and ET products derived from the MODerate resolution Imaging Spectroradiometer or MODIS aboard Terra and Aqua ^{18, 22}).

Several recently launched and forthcoming Earth-observing satellites have diurnal sampling capabilities. The recently launched ECOsystem Spaceborne Thermal Radiometer Experiment on Space Station (ECOSTRESS) and Orbiting Carbon Observatory-3 (OCO-3), both on board the

International Space Station (ISS), provide land surface temperature (LST), ET, and solar-induced chlorophyll fluorescence (SIF) data at different times of day. New generation geostationary satellites provide continuous observations throughout the day/night. Here we review these emerging satellite observations (Table 1) and explore the unprecedented opportunities for characterizing and understanding the diurnal cycling of plant functioning and ecosystem processes that have not yet been explored using measurements from space. We also envision how these emerging observations will revolutionize studies of plant functioning and ecosystem processes and how these observations and findings can inform agricultural management and improvement of Earth system models and climate projections.

Table 1. Specifications of the instruments/platforms that have diurnal sampling capability in studying plant functioning and ecosystem processes. NIR, SWIR, and TIR stand for near infrared, shortwave infrared, and thermal infrared wavelength, respectively.

Instrument	Platform	Launch date	Wavelength	Spatial	Repeat cycle	Spatial extent
				resolution		
ECOSTRESS	ISS	June 29, 2018	TIR	70 m	1-5days	Global (52°N
						- 52°S)
OCO-3	ISS	May 4, 2019	Far red, SWIR	2 km	~5days	Global (52°N
						- 52°S)
AHI	Himawari-8	October 7,	Visible, NIR,	0.5-2 km	10 mins ^a	Eastern Asia
		2014	SWIR, TIR			and Oceania
ABI	GOES-16	November 19,	Visible, NIR,	0.5-2 km	10 mins ^b	Western
		2016	SWIR, TIR			Hemisphere
ABI	GOES-17	March 1, 2018	Visible, NIR,	0.5-2 km	10 mins ^b	Western
		,	SWIR, TIR			Hemisphere
AGRI	Fengyun-4	December 10,	Visible, NIR,	0.5-4 km	15 mins	Eastern
	23	2016	SWIR, TIR			Hemisphere
FCI	MTG	≥2022	Visible, NIR,	0.5-2 km	10 mins ^c	Europe and
			SWIR, TIR			Africa
GeoCarb	TBD d	>2022	Far red, SWIR	5-10 km	<1 day	Americas
			,		5	(52°N - 52°S)
TEMPO	TBD ^d	≥2022	Red, far red	$2.1 \text{ km} \times 4.4$	Hourly	North
				km	J	America
UVN	Sentinel-4	≥2022	Visible, NIR	8 km	Hourly	Europe and
		_=	, 1			North Africa
						110111111111111111111111111111111111111

^a Himawari-8: 10 minutes for full disk and 2.5 minutes for Japan.

- 119 b GOES-16 and GOES-17: 10 minutes for full disk (with 15 minutes for full disk prior to April 2019), 5 minutes for
- the conterminous U.S, and 30 or 60 seconds at the mesoscale.
- 121 °MTG: 10 minutes for full disk (Europe and Africa) and 2.5 minutes for Europe.
- d TBD stands for "to be determined'. Both GeoCarb and TEMPO will be deployed on commercial geostationary
- 123 satellites.

124

125

ISS: ECOSTRESS

126 The ECOsystem Spaceborne Thermal Radiometer Experiment on Space Station (ECOSTRESS) 127 was launched to the International Space Station (ISS) by the National Aeronautics and Space 128 Administration (NASA) on 29 June 2018 ²³. ECOSTRESS measures thermal infrared radiation 129 (TIR) in five bands from 8- to 12.5-µm, plus an additional sixth band at 1.6 µm for geolocation 130 and cloud detection. ECOSTRESS covers the Earth continuously between ~52°N and ~52°S. 131 ECOSTRESS produces four levels of data products, with Levels 2-4 for primary science 132 applications. The pixel size at nadir is 38 m x 69 m, which is resampled to 70 m x 70 m pixels for higher level data products. The ECOSTRESS science products consist of LST and emissivity 133 (L2 LSTE) ^{24, 25}, ET including partitioning between canopy transpiration, soil evaporation, and 134 interception evaporation (L3 ET PT-JPL; L3 ET ALEXI) ^{23, 26}, and the Evaporative Stress Index 135 (ESI) and Water Use Efficiency (WUE) (Level 4) ^{27, 28}. LST is an instantaneous product, while 136 137 ET includes both instantaneous and daily estimates. Both ESI and WUE are currently daily 138 products. The daily WUE product is calculated from ECOSTRESS daily ET estimate and the 139 MODIS GPP product ¹⁸. Instantaneous WUE can be derived from the instantaneous ET estimates (e.g., L3 ET PT-JPL) ²³ and instantaneous GPP estimates ²⁹ based on ECOSTRESS LST data. 140 141 Field validation based on dozens of land sites showed that the ECOSTRESS LST product met the 142 accuracy requirement (daytime LST: bias = 0.1 K, RMSE = 1.1 K; nighttime LST: bias = -0.2 K; RMSE = 0.8 K) ³⁰. The ECOSTRESS ET product likewise performed well against in-situ 143 measurements from 82 EC flux sites ($R^2=0.88$, overall bias = 8%; normalized RMSE = 6%) ²³. 144

Flying in the precessing orbit of the ISS, ECOSTRESS collects measurements at different times of day, thereby sampling the diurnal cycle. The ISS orbit characteristics, in conjunction with the large 384-km ECOSTRESS swath width, enables a return frequency every 1–5 days, depending on latitude. Higher latitudes, where the ISS orbital direction shifts, are measured multiple times in a single day. ECOSTRESS therefore provides the highest combination of spatial and temporal resolution diurnal sampling of surface properties associated with temperature and water. ECOSTRESS can sample a large portion of the diurnal cycle over a period of weeks.

145

146

147

148

149

150

151

152

153

154

155

156

157

158

159

160

161

162

163

164

165

166

Diurnally, ECOSTRESS can provide transformative information about plant heat and water stress, and water use. While the diurnal sampling of geostationary satellites (e.g., Himawari-8, the GOES-R series) is more frequent, the coarse spatial resolution (e.g., 2 km for TIR bands) produces mixed pixels containing plant species or individuals with different diurnal cycles. The 70 m ECOSTRESS pixels are much closer to the scale of small ecosystem patches and individual agricultural fields. Further spatial downscaling is possible through fusion with other sensors ³¹. It is therefore possible to detect from space, for example, individual fields drying out in the afternoon (Fig. 2) — this has never been possible in the history of remote sensing before ECOSTRESS. This type of information can be returned to farmers and water managers who may not know that individual fields could use more water. Similarly, it may be possible to see parts of a forest drying out before other parts (e.g., forest edges) — again, information that can be critically useful for forest and fire managers. While diurnal water stress is certainly not a new phenomenon, until ECOSTRESS we did not know where and when this was occurring globally. This type of science application requires that satellite instruments offer observations with <100 m pixel size, <10% relative uncertainty, and <weekly repeat cycle.

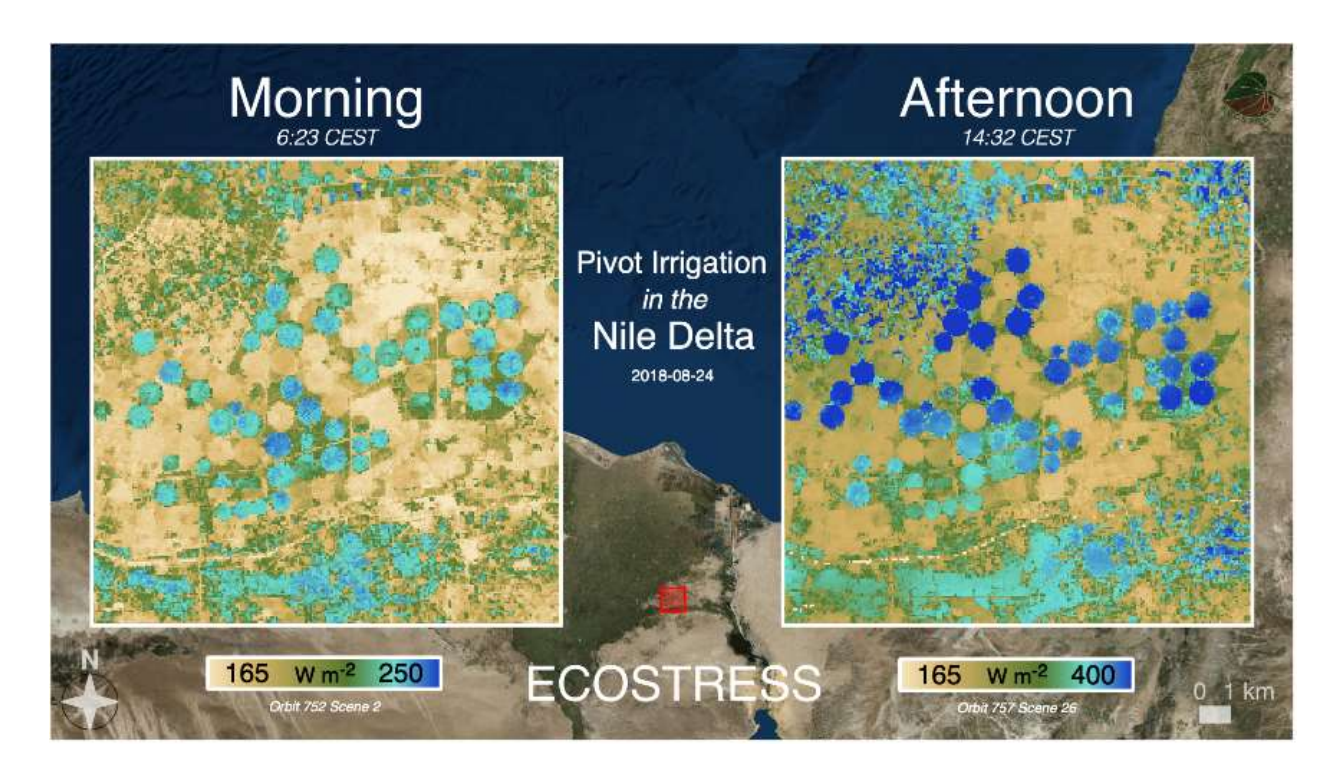


Fig. 2 NASA's ECOsystem Spaceborne Thermal Radiometer Experiment on Space Station (ECOSTRESS) imaged the Nile Delta, Egypt from the International Space Station in the morning and afternoon on August 24, 2018. ECOSTRESS captured changes in evapotranspiration (ET) from agricultural fields within the same day. The image on the left is from 6:23 CEST, and the image on the right is from 14:32 CEST. Much more ET is shown in the afternoon image (blue colors), though there are larger differences between the fields than in the morning. The geographical coordinates of the center of the ECOSTRESS images (Orbit 752, Scene 2 and Orbit 757, Scene 26) are 30.54° N and 31.85° E. The scale bar applies to the background map; the pixel size of the inset maps is 70 m.

From a plant ecophysiological perspective, we are interested in water-, temperature-, and vapor pressure deficit (VPD)-induced stomatal closure ³². We know well from local *in situ* measurements that some plants close stomata in response to these stressors ³³. However, not all plants behave the same even within the same area or species, for example, due to variations in rooting depth, soil moisture, and/or water table; and/or due to differences in species, age, and/or

disturbance history ³⁴. Although we know that these differences exist from local measurements, we do not know where these responses are occurring globally. That is where ECOSTRESS can advance plant ecophysiological science.

The suite of ECOSTRESS products can be used synergistically to understand diurnal cycle plant water and temperature responses. From the state-of-the-art number of TIR spectral bands and retrieval approach ³⁵, the LST data can map with great precision both the instantaneous heat of the plant surface as well as the duration that heat might extend into the day and night ²⁵. How that heat dissipates in time and space is related both to surface physical properties and water use (in the absence of exogenous factors). In turn, the ET data reveal how much water is used throughout the day, and how that water use deviates from expectations due to atmospheric demand alone ³⁶. The canopy transpiration product can be used to isolate the plant contribution to total ET ³⁷. The ESI product is useful for diagnosing attribution to ET responses, as well as lead-up prior to ET responses and drought impacts ³⁸. GPP estimates based on ECOSTRESS LST data can reveal how plant photosynthesis varies throughout the day in response to variations in environmental and physiological factors and management practices (e.g., irrigation) ²⁹. Finally, the WUE product can link water and temperature responses to carbon cycle processes ²⁸, as well as to synergistic measurements from other sensors, such as SIF from OCO-3 ³⁹.

ISS: OCO-3

The Orbiting Carbon Observatory-3 (OCO-3) was deployed to the ISS in May 2019, and has been collecting joint measurements of atmospheric CO₂ and plant SIF since August 2019 ⁴⁰. Unlike its polar orbiting predecessor (OCO-2) ⁴¹, OCO-3 samples reflected sunlight in the tropics and subtropics across the full range of daylight hours (dawn-to-dusk) with dense observations at northern and southern mid-latitudes (+/- 52°), like ECOSTRESS, due to the low-inclination ISS orbit. OCO-

3 also has a Snapshot Area Mode (SAM), and this technical innovation allows for localized mapping of SIF for the first time. By continuing the concurrent SIF observations of OCO-2 in time, expanding OCO-2 measurements in space, and focusing on ecosystem and urban hotspots, OCO-3 provides scientists a unique vantage of the processes that influence the global carbon cycle and plant behavior, thus increasing our understanding of how global climate patterns affect the terrestrial carbon cycle.

Plant fluorescence has been studied in laboratories and the field for several decades focusing on plant-level photosynthesis ⁴². When plants absorb solar energy for growth, they re-emit a small amount (~2%) of sunlight back to space. Although SIF exhibits a complex and varying relationship with photosynthesis at various scales (e.g., leaf, canopy, ecosystem) ^{43, 44}, ecosystem resolving spaceborne sensors such as GOME-2, GOSAT, OCO-2, and TROPOMI found a simple linear relationship between fluorescence and rates of ecosystem-scale photosynthesis observed at towers, nearly independent of vegetation type ^{21, 45, 46}. This allows scientists to use empirical relationships to estimate global rates of photosynthesis ⁴⁷, its change over time and space, and study its climate sensitivity (e.g., the photosynthesis of tropical continents responded in different ways to warming and drying during the 2015-16 El Niño) ⁴⁸. The intercomparison of SIF between OCO-3 and its predecessor (OCO-2) showed that OCO-3 SIF is of comparable quality as OCO-2 SIF ⁴⁰, which shows strong seasonal agreement with tower and airborne SIF measurements at a sub-alpine evergreen forest ⁴⁹, and correlates well with tower-based GPP across multiple biomes (with R² ranging from 0.73 to 0.81) ^{21, 45}.

While OCO-2 offers the high spectral resolution needed to capture the downregulation of photosynthesis under increasing water limitation ⁵⁰, it misses the full dynamic range of water stress responses due to fixed afternoon sampling during peak stress (~1:30 pm local). Moreover, attempts

to combine afternoon measurements from one polar-orbiting satellite (TROPOMI) with morning measurements from another satellite (GOME-2) reveal systematic orbital geometry-dependent variations which mask physiologically driven diurnal changes. A recent analysis of the FLUXNET2015 EC database shows that photosynthesis in most plant types typically peaks in late morning prior to peak potential shortwave incoming radiation, when water stress is low and boundary layer CO₂ is high, then decreases in the afternoon with lower light use efficiency ⁵¹. ET, meanwhile, typically peaks in the afternoon with VPD, creating diurnal hysteresis between ecosystem fluxes that is typically and critically unresolved by polar-orbiting satellites.

OCO-3 provides the diurnal sampling and spatial resolution needed to advance our understanding of photosynthesis especially under heat and water stress. OCO-3 passes over any given location (at nadir) ~20 minutes earlier each time, eventually sampling all sunlit hours ⁴⁰. Each time the instrument passes over, it collects SIF snapshots (1-2 km footprints) capable of resolving photosynthetic CO₂ uptake at the ecosystem. These measurements provide scientists with a new level of detail on the interaction between ecosystem scale photosynthetic processes and drought response.

OCO-3 target and SAM observations offer versatile alternatives to the narrow (~10 km) nadir and glint swaths for collection of dense, cloud-free, spatially resolved datasets at selected ecosystem hotspots and validation targets. OCO-3 scans a repeated swath over ~20 km x 20 km areas in the target mode and adjacent swaths over ~80 km x 80 km areas in the SAM mode. Target data are used primarily for CO₂ calibration and validation but offer high precision, diurnally and seasonally resolved SIF across a small subset of locations around the world. SAM data provide SIF across a wide variety of urban, volcanic, agricultural, and naturally vegetated locations to study biological exchange in managed and unmanaged landscapes. SAM locations can also be

reprogrammed for near-real time study of climate extremes (e.g., drought, flooding, fires), weather extremes (e.g., hurricane, derecho), and changes in management (e.g., irrigation, water-use restrictions).

The OCO-3 observations overlap in space and time with ECOSTRESS due to the shared ISS platform, although ECOSTRESS covers even more area due to its larger swath. A large percentage of SAM collection is coincident with ECOSTRESS priority EC validation sites. While the nature of the precessing ISS orbit can cause irregular spatial sampling, the extended spatial coverage enables more focused analyses of cloud-free subregions with overlapping coverage in time. For example, a series of SAMs collected at the Santa Rita Experimental Range in Arizona, USA demonstrate the impact of sporadic sampling and clouds on spatial maps (Fig. 3), but careful downsampling and quality control produces aggregated sounding and diurnal signature which resembles observations from ground-based measurements ^{49, 52, 53}. OCO-3, in combination with ECOSTRESS, provides cutting-edge insight into ecosystem processes of SIF and ET, and ultimately can be combined as WUE, with high resolution sampling throughout the day. While certainly an advance over predecessor measurements, both instruments still do not continuously observe the diurnal cycle, and therefore synergy with geostationary instruments can help close that loop.

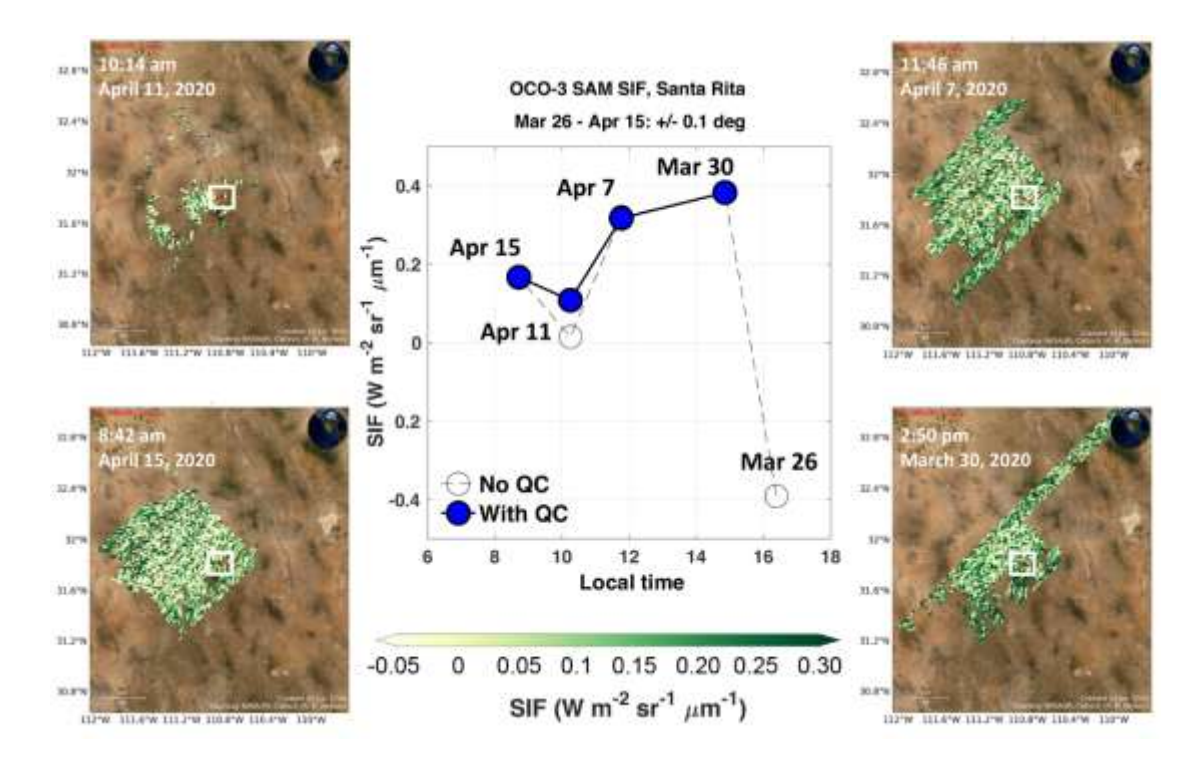


Fig. 3 Solar-induced chlorophyll fluorescence (SIF), a proxy of plant photosynthesis, at different times of day as measured by the Orbiting Carbon Observatory-3 (OCO-3) in the Snapshot Area Mapping (SAM) mode. The data were acquired surrounding the Santa Rita Experimental Range, Arizona (USA). The four maps show the spatial patterns of SIF at the landscape scale for different times of day in March and April, 2020. The center plot illustrates the diurnal variations of SIF spatially averaged within the 0.1 degree \times 0.1 degree area surrounding the Santa Rita Experimental Range research site, and only good-quality data (solar zenith angle < 70°, view zenith angle < 40°, cloud fraction < 0.1) were used.

New generation geostationary satellites

Although ECOSTRESS and OCO-3 have diurnal sampling capabilities, these samples are not continuous throughout the day for a given location. By contrast, geostationary satellites carry optical sensors with high-frequency observation capability (10 to 15 minutes in full scan mode). With such high temporal frequency and spectral features, these satellites are expected to improve diurnal monitoring of ecosystem dynamics ⁵⁴. Following the Himawari-8 (launched in 2014) with

the Advanced Himawari Imager (AHI) 55, the subsequent geostationary satellites carry the same type of optical sensors: Advanced Baseline Imager (ABI) on the Geostationary Operational Environmental Satellite-R Series (GOES-R) (GOES-16 launched in 2016 and GOES-17 launched in 2018) ⁵⁶ and Advanced Meteorological Imager (AMI) on GEO-KOMPSAT-2A (GK-2A) (launched in 2018) ⁵⁷. These instruments collect high-frequency observations of radiance in both solar reflective and TIR wavelengths. New sensors with similar features are also aboard China's and Europe's new generation geostationary satellites: Advanced Geostationary Radiation Imager (AGRI) on Fengyun-4 (FY-4) series (FY-4A was launched in 2016) 58 and Flexible Combined Imager (FCI) on Meteosat Third Generation (MTG) series ⁵⁹. The combination of the observations from those satellites (Table 1) can presumably cover the entire globe, and allow for the monitoring of any place on the Earth with such a high frequency. For example, the Copernicus Global Land Service (https://land.copernicus.eu) now provides LST data for a large portion of the Earth's land surface (Fig. S1 in the Supplementary Material). GeoNEX, a collaborative effort among NASA and agencies/organizations in other countries (e.g., Japan, Korea), is generating Earth monitoring products from the new generation geostationary satellites ⁶⁰.

283

284

285

286

287

288

289

290

291

292

293

294

295

296

297

298

299

300

301

302

303

304

305

TIR images with improved spectral, spatial, and temporal resolution can lead to more accurate and more frequent LST retrievals over previous geostationary measurements 61 . For example, the GOES-16 LST had good agreement with in-situ measurements (overall bias of -0.84 K 62), and the Himawari-8 LST was able to estimate LST with a RMSE \leq 0.9 K 61 . These observations can be used to understand how environmental stresses influence ET and GPP throughout the day. Furthermore, incoming solar radiation, which is a primary driver of photosynthesis, is available from geostationary satellites 63 . These geostationary satellite data can lead to high-frequency estimates of ecosystem processes throughout the day.

For example, we estimated hourly GPP over Australia at the hourly time step using the Himawari-8 AHI data and a light use efficiency model ⁶⁴ (Fig. 4). The meteorological input data, including solar radiation, air temperature, and VPD, were estimated from AHI visible and thermal bands and ground meteorological data using machine learning techniques. The MODIS Fraction of Absorbed Photosynthetically Active Radiation (FPAR) product ⁶⁵ was corrected using the normalized difference vegetation index (NDVI) time series derived from AHI. The comparison of the satellite-derived GPP to tower GPP from four EC flux sites showed consistent magnitude and diurnal patterns of hourly GPP (Figs. S2, S3). The resulting GPP product estimates gross carbon uptake of terrestrial ecosystems in Australia for each hour of the day. Fig. 4 illustrates how GPP varied over space for every two hours of the day and how GPP changed over the course of the day for each location across Northern Territory.

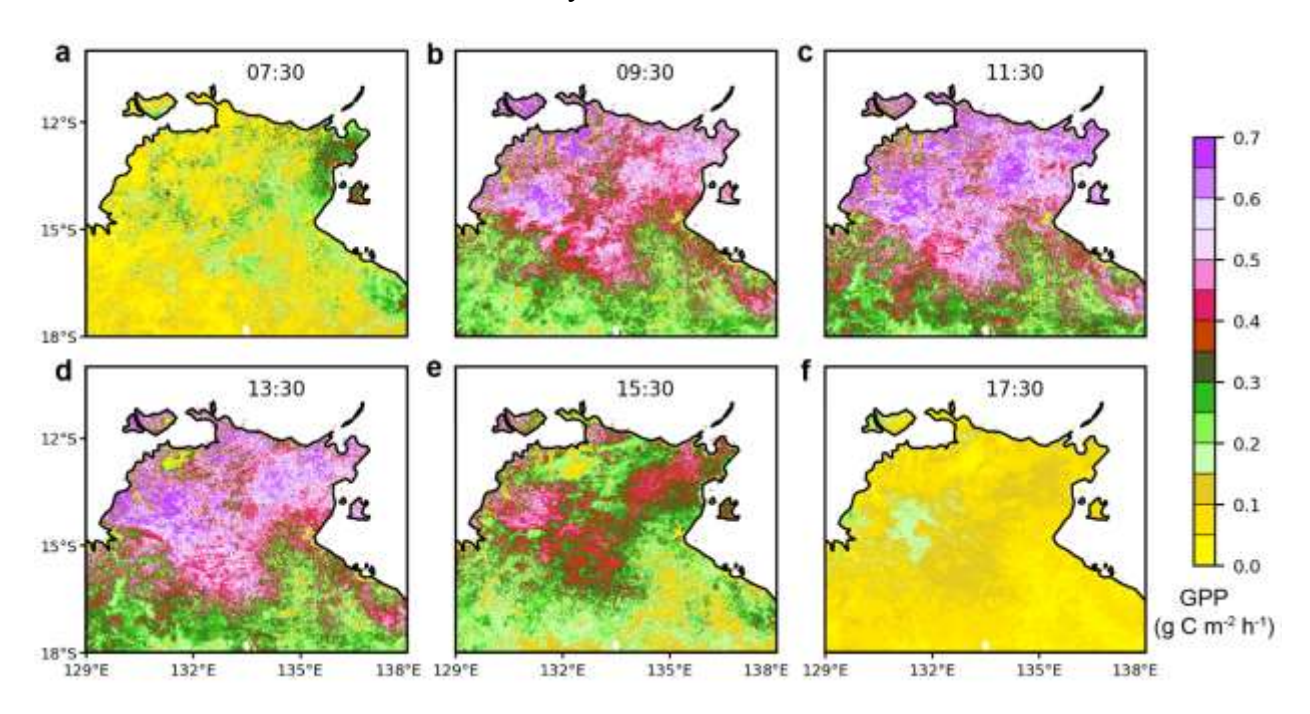


Fig. 4 Diurnal variations of plant photosynthesis (i.e., gross primary productivity, GPP) derived from geostationary satellite data (Himawari-8 AHI) and a light-use efficiency model. (a)-(f) show hourly GPP over Northern Territory, Australia every two hours from 7:30 to 17:30, Australian Central Time (ACT), on

February 1, 2018. The figure indicates that geostationary satellite data can be used to examine diurnal variations of ecosystem functioning.

323

324

325

326

327

328

329

330

331

332

333

334

335

336

337

338

339

340

341

342

343

344

322

321

Future missions

Some future missions also have planned diurnal sampling capabilities for ecosystem science (Table 1). The Geostationary Carbon Cycle Observatory (GeoCarb), a NASA mission with a currently planned launch as early as 2022, will measure CO₂, methane, carbon monoxide, and SIF ⁶⁶. GeoCarb will be hosted in geostationary orbit at 85°W, and will measure SIF over North and South America at 5-10 km resolution. GeoCarb will use O₂ and CO₂ channels that are similar to those used for the OCO-2, and will also use the OCO-2 algorithm for SIF retrieval. Whereas other SIF sensors have narrow swaths, GeoCarb can measure every pixel in a scan block in a few hours. In the block scan mode, GeoCarb can measure SIF at the same place only once or twice a day, like a sampler as opposed to a continuous recorder, depending on scan blocks. However, the flexible scan strategy of GeoCarb allows for the measurement of SIF at the target area multiple times a day by the intensive scan mode. NASA will also install the Tropospheric Emissions: Monitoring of Pollution (TEMPO) ⁶⁷ instrument on a commercial geostationary satellite in as early as 2022. TEMPO is mainly designed for monitoring air pollution but has the capability to measure SIF in both red and far-red wavelengths. TEMPO will cover North America with hourly frequency. However, the spectral resolution of TEMPO is coarse (0.6 nm), and therefore any SIF retrievals should be considered experimental. The European Space Agency (ESA) also has a planned similar geostationary mission, Sentinel-4, focusing on air pollution monitoring ⁶⁸. Sentinel-4 will cover Europe hourly with the Ultra-violet Visible Near-infrared (UVN) imaging spectrometer at 8 km resolution. Compared to OCO-3 that collects measurements globally between ~52°N and ~52°S, these future missions (i.e., GeoCarb, TEMPO, Sentinel-4) will provide SIF observations at the

continental scale. These SIF observations, when combined, will be valuable for capturing the diurnal variations of photosynthesis. With high frequency, TEMPO and Sentinel-4 missions can lead to increased cloud-free SIF retrievals. Although the combined use of the SIF data from these sensors can cover larger spatial domains, these SIF data will be based on different wavelengths and have different quality. In addition, SIF measured by geostationary satellite sensors can have a large range in the view zenith angle, and therefore the effects of view angle on SIF should be considered in analyses.

A small satellite (SmallSat) constellation can also potentially monitor the diurnal variations of vegetation status. SmallSats constellations have been well developed by commercial companies ⁶⁹, and some of them can be used for monitoring diurnal variations of ecosystem processes. For instance, Planet operates more than 100 SmallSats. Some of their satellite constellations, on an orbit similar to that of the ISS, can acquire observations for different times of day for each location with multiple optical bands and 0.5 - 3.7 m resolution ⁷⁰. Planet's SmallSats can be used to retrieve ET using the same algorithm as ECOSTRESS, as well as a fused Planet-ECOSTRESS retrieval, for example ⁷¹. Although these commercial satellite data are not free of charge, they provide increasing opportunities for studying ecosystem processes. A planned NASA SmallSats mission, Time-Resolved Observation of Precipitation structure and storm Intensity with a Constellation of Smallsats (TROPICS) ⁷², will consist of 12 CubeSats, and provide high-frequency (21 minutes) observations of temperature profile, humidity profile, and precipitation. TROPICS is not designed to monitor ecosystems but can contribute to the diurnal cycling analyses of ecosystem processes given the high frequency of the observations.

Studies on diurnal cycling of ecosystem functioning will also be able to greatly benefit from new ideas for missions that can integrate the advantages of these existing and forthcoming platforms. Ideally, such potential missions will be based on geostationary platforms but offer observations of LST with fine resolution equivalent to that of ECOSTRESS and observations of SIF with spatial resolution equivalent to that of OCO-3. While missions such as ECOSTRESS and OCO-3 are likely to continue well past their prime missions (e.g., ECOSTRESS is already an Extended Mission, having recently been approved for continuity in the NASA Senior Review), the shared platform of the ISS will perpetually introduce complex international negotiations over shared resources. So, new missions that can extend these types of measurements are still highly warranted. Still, the science and engineering communities must overcome current engineering limitations, costs, and tradeoffs associated with the high altitude geostationary orbits and the demand for high spatial, temporal, and spectral resolution.

Synergies

Emerging satellite diurnal observations can be synergistically used for new insights into plant functioning and ecosystem processes. ECOSTRESS and OCO-3, which normally would be unlikely pairs on the same mission platform, are now together afforded by the ISS. The combination of the data from these two instruments can allow us to examine plant transpiration and photosynthesis simultaneously and the coupling of these two processes for various types of ecosystems across the globe. Notably, the synergistic combination of OCO-3 SIF and ECOSTRESS ET can also provide a measure of WUE. Therefore, the synergistic use of ECOSTRESS and OCO-3 data can allow us to examine how plants use water and absorb carbon over the course of the diurnal cycle, and when, why, and how carbon and water uptake couple and decouple from one another. Fig. 5 illustrates the variations in SIF, ET, and WUE over a portion of the diurnal cycle at Santa Rita Experimental Range, Arizona (USA) based on ECOSTRESS and OCO-3 data acquired between March 26 – April 15, 2020. Although the coincident diurnal

measurements of ECOSTRESS and OCO-3 can directly provide diurnal measures of WUE that likely have lower uncertainty, it should be noted that OCO-3 does not offer wall-to-wall SIF coverage and also has coarse resolution, and that the combination of instantaneous ECOSTRESS ET estimates ²³ with instantaneous ECOSTRESS GPP estimates ²⁹ can lead to wall-to-wall and finer-resolution WUE estimates.

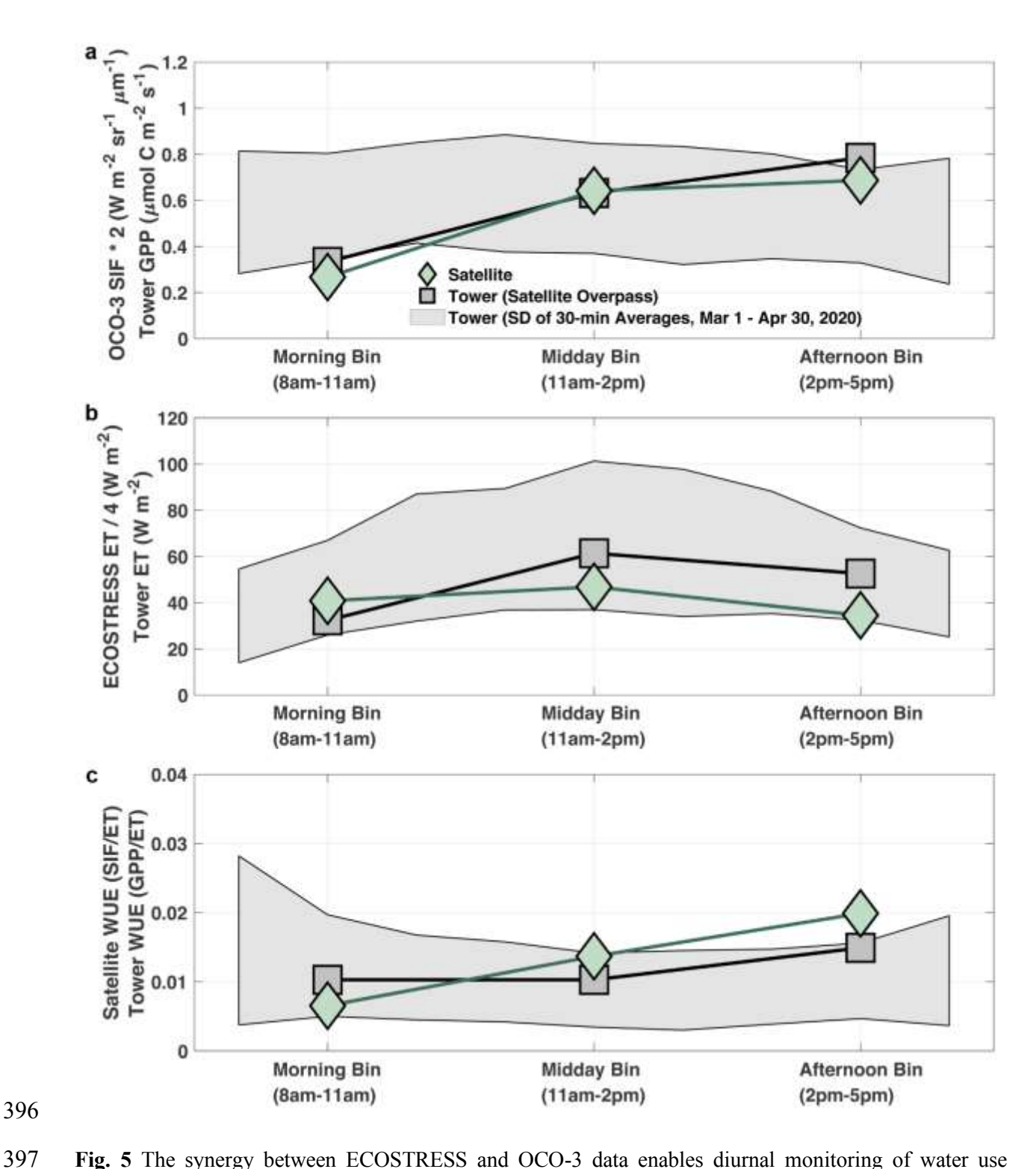


Fig. 5 The synergy between ECOSTRESS and OCO-3 data enables diurnal monitoring of water use efficiency (WUE) of terrestrial ecosystems. The ECOSTRESS ET, OCO-3 SIF (740 nm), and tower data at Santa Rita Experimental Range, Arizona, USA (31.82° E, 110.87° W) illustrate how OCO-3 SIF and

tower GPP (a), ECOSTRESS ET and tower ET (b), and satellite and tower WUE (c) vary over a portion of the diurnal cycle spanning morning, midday, and afternoon hours. Here satellite-derived WUE (W m⁻² sr⁻¹ μm⁻¹ / W m⁻²)_is defined as the ratio of SIF to ET, while tower-based WUE (μmol C m⁻² s⁻¹ / W m⁻²) is defined as the ratio of GPP to ET. The data were acquired between March 1 – April 30, 2020. The SIF and ET data were grouped into 3-hour bins (8-11 am, 11 am–2 pm, and 2-5 pm, local time) for the calculation of WUE.

406

407

408

409

410

411

412

413

414

415

416

417

418

419

420

421

422

423

400

401

402

403

404

405

Observations from ECOSTRESS and OCO-3 can also be synergistically used with data from geostationary satellites. ECOSTRESS and OCO-3 provide broader global-scale spatial coverage than any geostationary satellite, and therefore consistent studies of this scale are more straightforward from a single ISS platform than piecing together multiple satellites from different geostationary platforms. Despite the diurnal sampling capability, ECOSTRESS and OCO-3 provides only one or few (or no) observations for each location during a given day, and therefore capturing a large portion of the diurnal cycle will require ISS overpasses over a relatively long period (e.g., weeks). Over such a period of time, the variations in instantaneous LST, ET, or SIF are caused by not only diurnal variations in meteorological conditions and water/heat stress but also the day-to-day variations in these factors, vegetation structure (e.g., leaf area index or LAI), and/or phenology, which can complicate diurnal cycle analyses to a certain extent. Compared to these instruments, new-generation geostationary satellites (e.g., Himawari-8, the GOES-R series) provide continuous observations throughout the day. On the other hand, ECOSTRESS has much finer spatial resolution (70 m) than geostationary satellites (e.g., 2 km) and allows the identification of ecosystem patches or individual fields of croplands. The observations from these instruments can be synergistically used to study the diurnal variations of ecosystem processes by taking advantage of the temporally continuous nature of the geostationary satellite observations

throughout the day and the much finer spatial resolution of the ECOSTRESS data. With data fusion techniques e.g., ⁷³, the observations from these satellites/instruments can also potentially be merged to generate new data that are temporally continuous over the course of the day and also have fine spatial resolution.

424

425

426

427

428

429

430

431

432

433

434

435

436

437

438

439

440

441

442

443

444

445

446

As an illustration, the combined use of the data based on Himawari-8 AHI, ECOSTRESS, and OCO-3 allowed us to examine how plant photosynthesis and transpiration changed over the course of the day in response to heat and/or water stress in southern Australia (2018-2019 and 2019-2020) (Fig. 6). The AHI LST data covers the entire region (Fig. 6a) and beyond (Australia and eastern Asia). Compared with AHI, ECOSTRESS acquired a limited number of observations but offered much more spatial detail (Fig. 6b, c). The instantaneous ET estimates based on ECOSTRESS showed that with heat and water stress, grasslands and croplands (light green and brown areas) exhibited much lower ET in the early afternoon than in the early morning (~9 am); forests (bright green areas), with much higher elevation and deeper roots, had only slightly higher ET in the early afternoon than in the early morning (Fig. 6d, e). Meanwhile, SIF data from OCO-3 revealed differences in photosynthesis among different times of day and indicated that plants (in the area highlighted by the ellipse) had high photosynthesis in the early morning but had low values around 4:30 pm (Fig. 6f, g). Compared with the ISS instruments, AHI provides high-frequency observations throughout the day and makes it feasible to examine the full diurnal cycles of LST and GPP (Fig. 6h, i). The LST on the heatwave day exceeded 40 °C from ~9 am to ~6 pm and 60 °C from ~11 am to ~4 pm, and the stomatal closure due to water and heat stresses led to a substantial decline in transpiration and a large increase in canopy temperature (Fig. 6h). The hourly GPP based on AHI and the in-situ GPP based on an EC flux site showed large and rapid declines from late morning to the middle afternoon with the onset of heat stress over a four-day period (December 22-26, 2018) and exhibited mid-day depression (Fig. 6i). The AHI GPP captured the diurnal variations in EC GPP for both normal (R^2 =0.93, p<0.0001) and heatwave (R^2 =0.60, p<0.0001) days. This example indicates that we can explore diurnal cycling of ecosystem processes from space using these unique datasets together.

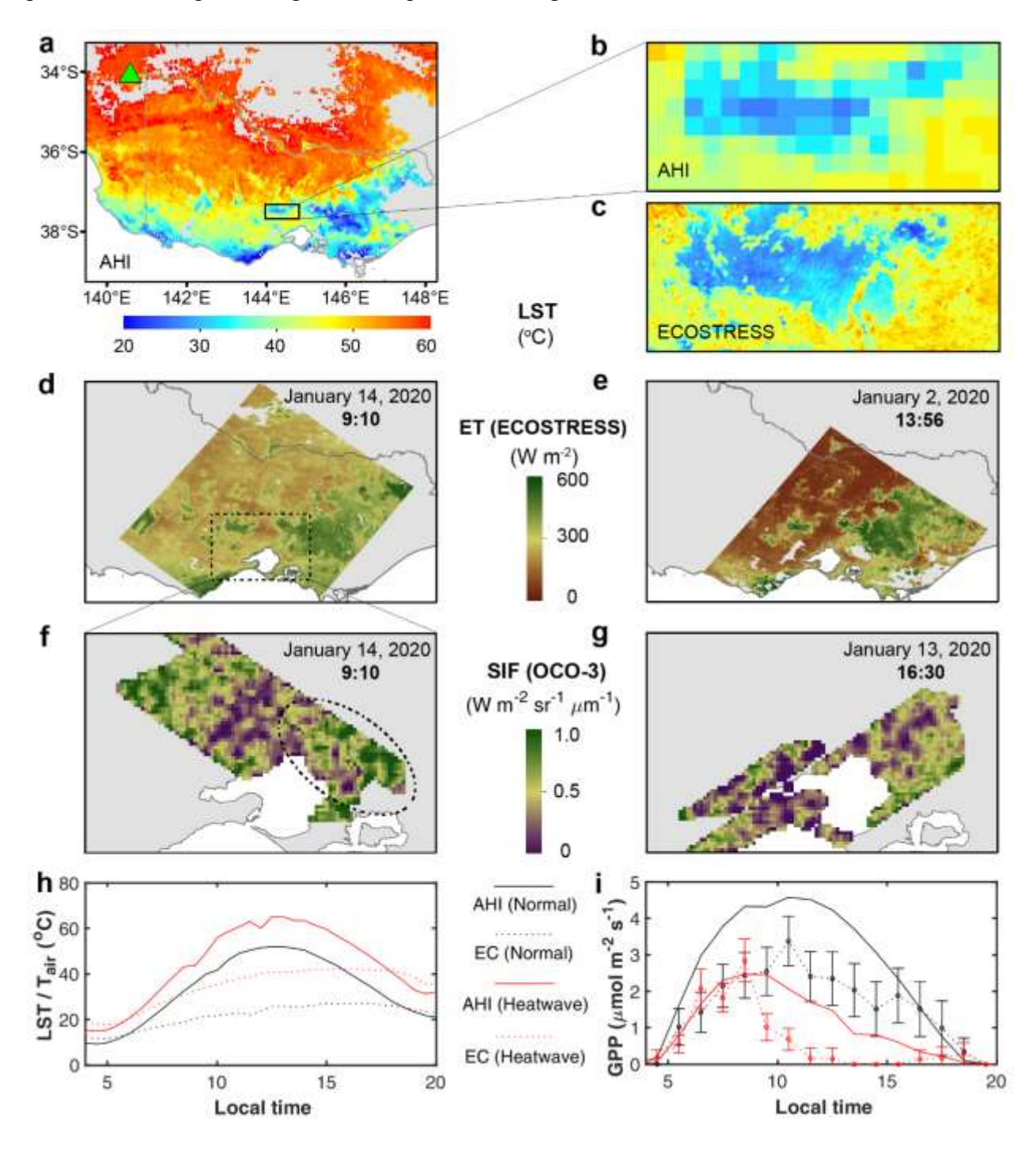


Fig. 6 Synergistic use of observations from a geostationary satellite instrument (Himawari-8 AHI) and two instruments from the International Space Station (ECOSTRESS and OCO-3) for studying diurnal cycling of ecosystem processes during heatwaves over Australia's summers (2018 and 2020). (a) shows AHI LST at 13:30, January 2, 2020 for southern Australia and the location of the eddy covariance (EC) flux site (Calperum Chowilla, location indicated by the green symbol in a), while (b) and (c) show the coarse-resolution AHI LST and fine-resolution ECOSTRESS LST (13:55, January 2, 2020) for the small area as highlighted by the rectangle in (a). (d) and (e) are instantaneous ECOSTRESS ET for different times of day. (f) and (g) are instantaneous OCO-3 SIF for different times of day, and the highlighted area with an ellipse exhibits relatively high SIF in the early morning but low values in the late afternoon. (h) illustrates diurnal variations in LST (AHI) and air temperature (T_{air}) for a normal day (December 22, 2018) and a heatwave day (December 26, 2018) at the EC site, and (i) shows diurnal variations in AHI-based GPP estimates and flux tower GPP for both the normal and heatwave days at the EC site; the error bars indicate the uncertainty associated with flux partitioning. All times are local time.

The observations from ECOSTRESS, OCO-3, and new generation geostationary satellites also have anticipated synergies with those from the forthcoming missions. For example, the SIF data from OCO-3 and GeoCarb can be directly integrated for ecosystem studies over the Americas. Taken together, the observations from these two missions will cover a 13-18 year period starting from 2019, allowing continued exploration of diurnal photosynthesis at interannual and decadal scales. For example, this will make it possible to examine how the increasing atmospheric CO₂ concentrations influence stomatal behavior and plant photosynthesis. The SIF data from OCO-3, GeoCarb, and TEMPO can also be synergistically used by taking advantage of the higher-quality data from OCO-3 and GeoCarb and high-frequency measurements from TEMPO.

Besides the synergies among these emerging observations, these data can also be used in combination with data from polar-orbiting satellites (e.g., Terra, Aqua, Suomi NPP, JPSS, Landsat,

Sentinel, OCO-2, SmallSats) and in-situ measurements. Polar-orbiting satellites provide observations of vegetation for the globe over multiple decades. These data products (e.g., vegetation indices, LAI) can be used to provide additional essential variables or extend spatial or temporal domains for the diurnal cycle analyses based on the emerging observations with diurnal sampling capability. Moreover, because of the polar orbit, the Terra and Aqua have significant swath overlap at the high latitudes (e.g., the Arctic), and the resulting larger number of observations can potentially be used for diurnal cycling studies.

477

478

479

480

481

482

483

484

485

486

487

488

489

490

491

492

493

494

495

496

497

498

In-situ measurements have been traditionally used to study diurnal cycling of ecological and physiological processes. For example, previous studies used leaf-level measurements to understand the responses of stomata, leaf photosynthesis, and transpiration to soil water content, leaf water potential, and VPD ^{5, 33} and midday depression of photosynthesis ⁷⁴. Ground measurement networks for water, carbon, and energy fluxes such as FLUXNET 17 and the National Ecological Observatory Network (NEON) ⁷⁵ provide continuous half-hourly measurements and ancillary ecological and environmental data. These data have been used to examine the diurnal cycling of ecological and physiological processes, such as the influences of heat and water stresses on canopy conductance, ET, GPP, and WUE ¹⁶, physiological responses of carbon-water coupling to hydraulic and non-stomatal limitations ¹⁵, and hysteresis patterns of ET and GPP ⁵¹. The emerging satellite observations for diurnal cycling of ecosystem processes make it feasible to explore these ecophysiological processes and phenomena at expanded spatial scales (e.g., ecosystems, regions, the globe) from space. Ecophysiological understanding based on in-situ measurements will inform and facilitate the exploration of plant water stress and carbon uptake at the regional to global scales using the measurements from space. Data from ECOSTRESS, OCO-

3, and the new generation geostationary satellites can be directly linked with half-hourly or hourly flux data to quantify GPP, ET, and/or WUE over regions or the globe for different times of day.

Conclusions

499

500

501

502

503

504

505

506

507

508

509

510

511

512

513

514

515

516

517

518

519

Diurnal cycling of ecosystem processes is of significant scientific importance for understanding plant water use and carbon uptake in response to water and heat stress, changing climate, rising atmospheric CO₂, and management practices. We envision that the emerging satellite observations outlined in this article will trigger numerous research efforts aimed at understanding how plant carbon uptake and water use vary over the course of the diurnal cycle from ecosystem to the globe. Data from ECOSTRESS, OCO-3, geostationary satellites, and future missions with diurnal sampling capability (e.g., GeoCarb, TEMPO, Sentinel-4) are anticipated to be used both individually and synergistically. These observations will likely revolutionize studies of ecosystem processes and carbon and water cycling to a certain extent. The resulting analyses can help us better understand the resilience and vulnerability of different ecosystem types to drought and heat waves. For croplands, these data can reveal how plant water use varies throughout the day and how irrigation influences ET, water stress, and photosynthesis, and the findings can inform agricultural management (e.g., irrigation strategies). The instantaneous estimates of ecosystem processes at regional to global scales over the course of the diurnal cycle will be useful for calibrating and validating Earth system models. Better understanding how ecosystem processes respond to water and heat stress, changing climate, and rising atmospheric CO₂ with the emerging satellite observations can also guide the improvement of Earth system models and projections of carbon/water dynamics and carbon-climate feedbacks.

520

521

References:

Hennessey T. L., Freeden A. L., Field C. B. Environmental effects on circadian rhythms in photosynthesis and stomatal opening. *Planta* **189**, 369-376 (1993).

524

533

536

540

544

548

552

556

559

- 525 2. Steed G., Ramirez D. C., Hannah M. A., Webb A. A. R. Chronoculture, harnessing the circadian clock to improve crop yield and sustainability. *Science* **372**, eabc9141 (2021). 527
- Zhao T. B., Dai A. G. The Magnitude and Causes of Global Drought Changes in the Twenty First Century under a Low-Moderate Emissions Scenario. *J Clim* 28, 4490-4512 (2015).
- Perkins-Kirkpatrick S. E., Gibson P. B. Changes in regional heatwave characteristics as a function of increasing global temperature. *Scientific Reports* **7**, (2017).
- 534 5. Bates L. M., Hall A. E. Stomatal closure with soil-water depletion not associated with changes in bulk leaf water status. *Oecologia* **50**, 62-65 (1981).
- Roessler P. G., Monson R. K. Midday depression in net photosynthesis and stomatal conductance in Yucca-Glauca relative contributions of leaf temperature and leaf-to-air water-vapor concentration difference. *Oecologia* **67**, 380-387 (1985).
- 541 7. Tenhunen J. D., Pearcy R. W., Lange O. L. Diurnal variations in leaf conductance and gas 542 exchange in natural environments. In: *Stomatal Function* (eds Zeiger E, Farquhar GD, 543 Cowan IR). Stanford University Press (1987).
- 545 8. Tucci M. L. S., Erismann N. M., Machado E. C., Ribeiro R. V. Diurnal and seasonal variation in photosynthesis of peach palms grown under subtropical conditions. *Photosynthetica* **48**, 421-429 (2010).
- 549 9. Kosugi Y., Matsuo N. Seasonal fluctuations and temperature dependence of leaf gas exchange parameters of co-occurring evergreen and deciduous trees in a temperate broad-leaved forest. *Tree Physiol* **26**, 1173-1184 (2006).
- 553 10. Koch G. W., Amthor J. S., Goulden M. L. Diurnal patterns of leaf photosynthesis, conductance and water potential at the top of a lowland rain-forest canopy in Cameroon measurements from the Radeau-Des-Cimes. *Tree Physiol* **14**, 347-360 (1994).
- 557 11. Olioso A., Carlson T. N., Brisson N. Simulation of diurnal transpiration and photosynthesis of a water stressed soybean crop. *Agric For Meteorol* **81**, 41-59 (1996).
- 560 12. Cowan I. R., Farquhar G. D. Stomatal function in relation to leaf metabolism and environment: Stomatal function in the regulation of gas exchange. *Symposia of the Society for Experimental Biology* **31**, 471-505 (1977).
- Bollig C., Feller U. Impacts of drought stress on water relations and carbon assimilation in grassland species at different altitudes. *Agric Ecosyst Environ* **188**, 212-220 (2014).

566
 567
 14. Koyama K., Takemoto S. Morning reduction of photosynthetic capacity before midday depression. *Scientific Reports* 4, (2014).

569

580

588

592

595

599

602

- 570 15. Nelson J. A., Carvalhais N., Migliavacca M., Reichstein M., Jung M. Water-stress-induced 571 breakdown of carbon-water relations: indicators from diurnal FLUXNET patterns. 572 *Biogeosciences* **15**, 2433-2447 (2018). 573
- 574 16. Xu H., Xiao J. F., Zhang Z. Q. Heatwave effects on gross primary production of northern 575 mid-latitude ecosystems. *Environmental Research Letters* **15**, (2020). 576
- 577 17. Baldocchi D., *et al.* FLUXNET: A new tool to study the temporal and spatial variability of ecosystem-scale carbon dioxide, water vapor, and energy flux densities. *Bull Amer Meteorol Soc* **82**, 2415-2434 (2001).
- 581 18. Running S. W., Nemani R. R., Heinsch F. A., Zhao M. S., Reeves M., Hashimoto H. A continuous satellite-derived measure of global terrestrial primary production. *Bioscience* 583 54, 547-560 (2004).
- 585 19. Xiao J. F., et al. A continuous measure of gross primary production for the conterminous United States derived from MODIS and AmeriFlux data. *Remote Sens Environ* **114**, 576-587 591 (2010).
- 589 20. Anderson M. C., Allen R. G., Morse A., Kustas W. P. Use of Landsat thermal imagery in monitoring evapotranspiration and managing water resources. *Remote Sens Environ* **122**, 591 50-65 (2012).
- 593 21. Sun Y., et al. OCO-2 advances photosynthesis observation from space via solar-induced chlorophyll fluorescence. *Science* **358**, (2017).
- 596 22. Mu Q., Heinsch F. A., Zhao M., Running S. W. Development of a global evapotranspiration algorithm based on MODIS and global meteorology data. *Remote Sens Environ* **111**, 519-598 536 (2007).
- 600 23. Fisher J. B., et al. ECOSTRESS: NASA's Next Generation Mission to Measure Evapotranspiration From the International Space Station. Water Resour Res **56**, (2020).
- 603 24. Hook S. J., et al. In-flight validation of ECOSTRESS, Landsat 7 and 8 Thermal Infrared Spectral Channels using the Lake Tahoe CA/NV and Salton Sea CA Automated Validation Sites. *IEEE Transactions on Geoscience and Remote Sensing* **58**, 1294-1302 (2019).
- 607 25. Hulley G., Shivers S., Wetherley E., Cudd R. New ECOSTRESS and MODIS land surface 608 temperature data reveal fine-scale heat vulnerability in cities: A case study for Los Angeles 609 County, California. *Remote Sensing* **11**, 2136 (2019).

610
611
26. Anderson M. C., et al. Interoperability of ECOSTRESS and Landsat for mapping evapotranspiration time series at sub-field scales. Remote Sens Environ 252, (2021).

613

Anderson M. C., et al. An Intercomparison of Drought Indicators Based on Thermal Remote Sensing and NLDAS-2 Simulations with US Drought Monitor Classifications. J Hydrometeorol 14, 1035-1056 (2013).

617

618 28. Cooley S. S., Fisher J. B., Halverson G. H., Goldsmith G. R. A new satellite-based measure 619 of water use efficiency reveals convergence within global plant functional types across 620 climates. *Nature Plants*, in revision (2021).

621

422 29. Li X., Xiao J., Fisher J. B., Baldocchi D. D. ECOSTRESS estimates gross primary production
 with fine spatial resolution for different times of day from the International Space Station.
 Remote Sens Environ 258, 112360 (2021).

625

30. Hulley G., Freepartner R., Radocinski R. Level-2 Land Surface Temperature and Emissivity.
 In: ECOSTRESS Science Team Meeting) (2019).

628

Aragon B., Houborg R., Tu K., Fisher J. B., McCabe M. CubeSats Enable High Spatiotemporal Retrievals of Crop-Water Use for Precision Agriculture. *Remote Sensing* 10, 1867 (2018).

632

633 32. Fisher J. B., *et al.* The future of evapotranspiration: Global requirements for ecosystem functioning, carbon and climate feedbacks, agricultural management, and water resources. *Water Resources Research* **53**, 2618-2626 (2017).

636

Turner N. C., Schulze E.-D., Gollan T. The responses of stomata and leaf gas exchange to vapour pressure deficits and soil water content. *Oecologia* **65**, 348-355 (1985).

639

Moore G. W., Heilman J. L. Proposed principles governing how vegetation changes affect transpiration. *Ecohydrology* **4**, 351-358 (2011).

642

Hulley G. C., Hook S. J. Generating consistent land surface temperature and emissivity products between ASTER and MODIS data for earth science research. *Geoscience and Remote Sensing, IEEE Transactions on* **49**, 1304-1315 (2011).

646

647 36. Fisher J. B., Whittaker R. H., Malhi Y. ET Come Home: A critical evaluation of the use of evapotranspiration in geographical ecology. *Global Ecology and Biogeography* **20**, 1-18 (2011).

650

Talsma C. J., et al. Partitioning of evapotranspiration in remote sensing-based models.

Agricultural and Forest Meteorology **260**, 131-143 (2018).

- 654 38. Otkin J. A., Anderson M. C., Hain C., Mladenova I. E., Basara J. B., Svoboda M. Examining 655 Rapid Onset Drought Development Using the Thermal Infrared—Based Evaporative Stress 656 Index. *Journal of Hydrometeorology* **14**, 1057-1074 (2013).
- 657
 658 39. Stavros E. N., et al. ISS observations offer insights into plant function. *Nature Ecology & Evolution* 1, 1-4 (2017).

660

667

671

675

682

686

690

- 661 40. Taylor T. E., et al. OCO-3 early mission operations and initial (vEarly) XCO2 and SIF retrievals. Remote Sens Environ **251**, 112032 (2020).
- 664 41. Frankenberg C., et al. The Orbiting Carbon Observatory (OCO-2): spectrometer performance evaluation using pre-launch direct sun measurements. Atmos Meas Tech 8, 301-313 (2015).
- 668 42. Bilger W., Schreiber U., Bock M. Determination of the quantum efficiency of photosystem-669 II and of nonphotochemical quenching of chlorophyll fluorescence in the field. *Oecologia* 670 **102**, 425-432 (1995).
- 672 43. Maguire A. J., et al. On the Functional Relationship Between Fluorescence and Photochemical Yields in Complex Evergreen Needleleaf Canopies. *Geophys Res Lett* **47**, 674 (2020).
- 676 44. Marrs J. K., et al. Solar-Induced Fluorescence Does Not Track Photosynthetic Carbon 677 Assimilation Following Induced Stomatal Closure. *Geophys Res Lett* **47**, (2020).
- Li X., et al. Solar-induced chlorophyll fluorescence is strongly correlated with terrestrial photosynthesis for a wide variety of biomes: First global analysis based on OCO-2 and flux tower observations. Glob Change Biol 24, 3990-4008 (2018).
- 683 46. Frankenberg C., et al. New global observations of the terrestrial carbon cycle from GOSAT:
 684 Patterns of plant fluorescence with gross primary productivity. Geophys Res Lett 38,
 685 (2011).
- 687 47. Li X., Xiao J. F. Mapping Photosynthesis Solely from Solar-Induced Chlorophyll 688 Fluorescence: A Global, Fine-Resolution Dataset of Gross Primary Production Derived 689 from OCO-2. *Remote Sens* **11**, (2019).
- 691 48. Liu J. J., et al. Contrasting carbon cycle responses of the tropical continents to the 2015-692 2016 El Nino. *Science* **358**, 191-+ (2017).
- 694 49. Parazoo N. C., et al. Towards a Harmonized Long-Term Spaceborne Record of Far-Red Solar-Induced Fluorescence. *J Geophys Res* **124**, 2518-2539 (2019).

- 697 50. He L. Y., et al. Tracking Seasonal and Interannual Variability in Photosynthetic 698 Downregulation in Response to Water Stress at a Temperate Deciduous Forest. *J Geophys* 699 *Res* **125**, (2020).
- 51. Lin C. J., Gentine P., Frankenberg C., Zhou S., Kennedy D., Li X. Evaluation and mechanism exploration of the diurnal hysteresis of ecosystem fluxes. *Agric For Meteorol* **278**, (2019).

700

713

717

724

- 704 52. Magney T. S., et al. Mechanistic evidence for tracking the seasonality of photosynthesis with solar-induced fluorescence. *Proc Natl Acad Sci U S A* **116**, 11640-11645 (2019). 706
- 707 53. Yang X., et al. FluoSpec 2-An Automated Field Spectroscopy System to Monitor Canopy 708 Solar-Induced Fluorescence. Sensors-Basel 18, (2018).
- 710 54. Miura T., Nagai S., Takeuchi M., Ichii K., Yoshioka H. Improved Characterisation of Vegetation and Land Surface Seasonal Dynamics in Central Japan with Himawari-8 Hypertemporal Data. *Scientific Reports* **9**, (2019).
- Bessho K., et al. An Introduction to Himawari-8/9-Japan's New-Generation Geostationary
 Meteorological Satellites. Journal of the Meteorological Society of Japan 94, 151-183
 (2016).
- Schmit T. J., Griffith P., Gunshor M. M., Daniels J. M., Goodman S. J., Lebair W. J. A closer
 look at the ABI on the GOES-R series. *Bull Amer Meteorol Soc* 98, 681-698 (2017).
- 721 57. Oh S. M., Borde R., Carranza M., Shin I. C. Development and Intercomparison Study of an Atmospheric Motion Vector Retrieval Algorithm for GEO-KOMPSAT-2A. *Remote Sens* **11**, 723 (2019).
- 725 58. Yang J., Zhang Z. Q., Wei C. Y., Lu F., Guo Q. Introducing the new generation of Chinese geostationary weather satellites, Fengyun-4. *Bull Amer Meteorol Soc* **98**, 1637-1658 (2017).
- Ouaknine J., et al. The FCI on board MTG: optical design and performances. In:
 International Conference on Space Optics-Icso 2014 (eds Sodnik Z, Cugny B, Karafolas N).
 Spie-Int Soc Optical Engineering (2014).
- 733 60. Wang W. L., *et al.* An Introduction to the Geostationary-NASA Earth Exchange (GeoNEX) 734 Products: 1. Top-of-Atmosphere Reflectance and Brightness Temperature. *Remote Sens* 735 **12**, (2020).
- 737 61. Yamamoto Y., Ishikawa H., Oku Y., Hu Z. Y. An Algorithm for Land Surface Temperature 738 Retrieval Using Three Thermal Infrared Bands of Himawari-8. *Journal of the* 739 *Meteorological Society of Japan* **96B**, 59-76 (2018). 740

741 62. Yu Y., Yu P. Chapter 12 - Land Surface Temperature Product from the GOES-R Series. In: 742 The GOES-R Series. A New Generation of Geostationary Environmental Satellites) (2020).

743

746

750

753

757

760

764

768

- 744 63. Takenaka H., et al. Estimation of solar radiation using a neural network based on radiative transfer. *J Geophys Res* **116**, (2011).
- 747 64. Hashimoto H., Wang W., Michaelis A., Takenaka H., Higuchi A., Nemani R. R. Hourly GPP
 748 Estimation in Australia Using Himawari-8 AHI Products. In: *IGARSS 2020 2020 IEEE*749 *International Geoscience and Remote Sensing Symposium*) (2020).
- 751 65. Yan K., et al. Evaluation of MODIS LAI/FPAR Product Collection 6. Part 1: Consistency and Improvements. *Remote Sens* **8**, (2016).
- 754 66. Moore B., et al. The Potential of the Geostationary Carbon Cycle Observatory (GeoCarb) 755 to Provide Multi-scale Constraints on the Carbon Cycle in the Americas. Frontiers in 756 Environmental Science 6, (2018).
- 758 67. Zoogman P., et al. Tropospheric emissions: Monitoring of pollution (TEMPO). *Journal of Quantitative Spectroscopy & Radiative Transfer* **186**, 17-39 (2017).
- 761 68. Courrèges-Lacoste G. B., et al. Knowing what we breathe: Sentinel 4: a geostationary imaging UVN spectrometer for air quality monitoring. In: *International Conference on Space Optics ICSO 2016* (ed Karafolas N, Cugny, B. & Sodnik, Z.) (2017).
- 765 69. Wekerle T., Pessoa J. B., da Costa L., Trabasso L. G. Status and Trends of Smallsats and their Launch Vehicles An up-to-date Review. *Journal of Aerospace Technology and Management* **9**, 269-286 (2017).
- 769 70. Ryswyk M. V. Planet announces 50 cm SkySat imagery, tasking dashboard and up to 12x revisit.). https://www.planet.com/pulse/tasking-dashboard-50cm-12x-revisit-announcement/ (2020).
- 773 71. Aragon B., Houborg R., Tu K., Fisher J. B., McCabe M. CubeSats Enable High Spatiotemporal Retrievals of Crop-Water Use for Precision Agriculture. *Remote Sens* **10**, 775 (2018).
- 777 72. Blackwell W. J., et al. An overview of the TROPICS NASA Earth Venture Mission. *Q J R*778 *Meteorol Soc* **144**, 16-26 (2018).
 779
- 73. Gao F., Masek J., Schwaller M., Hall F. On the blending of the Landsat and MODIS surface reflectance: Predicting daily Landsat surface reflectance. *IEEE Trans Geosci Remote Sensing* **44**, 2207-2218 (2006).

- 74. Franco A. C., Luttge U. Midday depression in savanna trees: coordinated adjustments in photochemical efficiency, photorespiration, CO2 assimilation and water use efficiency. *Oecologia* **131**, 356-365 (2002).
- 75. Keller M., Schimel D. S., Hargrove W. W., Hoffman F. M. A continental strategy for the National Ecological Observatory Network. *Front Ecol Environ* **6**, 282-284 (2008).

793 Acknowledgements

787

791 792

810

794 This study was supported by the National Aeronautics and Space Administration (NASA)'s 795 ECOSTRESS Science and Applications Team (80NSSC20K0167) (J.X.), NASA's Climate 796 Indicators and Data Products for Future National Climate Assessments (NNX16AG61G) (J.X.), 797 National Science Foundation (Macrosystem Biology & NEON-Enabled Science program: DEB-798 2017870) (J.X.), NASA's ECOSTRESS (J.B.F.), NASA Earth Exchange (NEX) from NASA's 799 Earth Science Division (H.H.), the Virtual Laboratory (VL) project by the Ministry of Education, 800 Culture, Sports, Science and Technology (MEXT), Japan (K.I.), a research grant of the Japan 801 Society for the Promotion of Science (JSPS), KAKENHI (20K20487) (K.I.), and the Earth Science Division OCOST program (N.C.P.). J.B.F. and N.C.P. carried out their research at the Jet 802 803 Propulsion Laboratory, California Institute of Technology, under a contract with the National 804 Aeronautics and Space Administration. California Institute of Technology. Government 805 sponsorship acknowledged. A portion of these data were produced by the OCO-3 project at the Jet 806 Propulsion Laboratory, California Institute of Technology, and obtained from the OCO-3 data 807 archive at the NASA Goddard Earth Science Data and Information Services Center. Gregory 808 Halverson provided ECOSTRESS visualization. Himawari-8 AHI based LST data used in this 809 study were provided by Dr. Y. Yamamoto, Chiba University, Japan.

311	Authors contributions
812	J.X. conceived the idea. J.X., J.B.F., H.H., K.I., and N.C.P. designed the research, conducted the
313	analyses, interpreted the data, and wrote the paper.
814	
815	Competing interests
816	The authors declare no competing interests.
817	
818	Data availability statement
819	The data that support the findings of this study are available from https://earthdata.nasa.gov
320	(ECOSTRESS), https://lpdaacsvc.cr.usgs.gov/appeears/ (ECOSTRESS)
321	https://ocov3.jpl.nasa.gov/oco-3-data-center/ (OCO-3), http://data.ozflux.org.au (flux tower data)
322	https://data.nas.nasa.gov/geonex/ (Himawari-8), ftp://hmwr829gr.cr.chiba-riches-riche
823	u.ac.jp/gridded/FD/V20151105/ (Himawari-8), and https://land.copernicus.eu/global/products/
324	(global geostationary satellite LST data)